European Journal of Environmental and Civil Engineering

ISSN: 1964-8189 (Print) 2116-7214 (Online) Journal homepage: https://www.tandfonline.com/loi/tece20

Artificial neural network for the prediction of the steel–concrete bond behaviour

Moncef Makni, Atef Daoud, Mohamed Ali Karray & Michel Lorrain

To cite this article: Moncef Makni, Atef Daoud, Mohamed Ali Karray & Michel Lorrain (2014) Artificial neural network for the prediction of the steel–concrete bond behaviour, European Journal of Environmental and Civil Engineering, 18:8, 862-881, DOI: 10.1080/19648189.2014.909745

To link to this article: https://doi.org/10.1080/19648189.2014.909745

Published online: 08 May 2014.

Submit your article to this journal

Article views: 238

View related articles

View Crossmark data

Citing articles: 5 View citing articles

Full Terms & Conditions of access and use can be found at
https://www.tandfonline.com/action/journalInformation?journalCode=tece20

European Journal of Environmental and Civil Engineering, 2014
Vol. 18, No. 8, 862–881, http://dx.doi.org/10.1080/19648189.2014.909745

Taylor & Francis
Taylor & Francis

Artificial neural network for the prediction of the steel–concrete bond behaviour

Moncef Makni[a,b], Atef Daoud[a,c]*, Mohamed Ali Karray[a] and Michel Lorrain[d,e]

[a]*Laboratoire de Génie Civil, Université de Tunis El MANAR, Tunis, Tunisia;* [b]*Institut Supérieur des Etudes Technologiques de Sfax, Sfax, Tunisia;* [c]*ENIG, Université de Gabès, Gabès, Tunisia;* [d]*INSA, Université de Toulouse, Toulouse, France;* [e]*SIAME, Université de Pau et des Pays de l'Adour, Pau, France*

(*Received 17 September 2012; accepted 26 March 2014*)

This paper aimed to show possible applicability of artificial neural networks (ANN) to predict the performance of the bond between reinforcement and concrete. An ANN model is constructed, trained and tested using the available test data of 117 different pull-out cylindrical concrete specimens with an embedded reinforcing bar. The data used in ANN model are arranged in a format of four input parameters that cover the concrete compressive strength, cover thickness, embedment length and related rib area. The ANN model, which performs in Matlab software, predicts the bond strength of anchoring capacity of the reinforcement in the concrete. The results showed that ANNs have strong potential as a feasible tool for predicting bond strength. Comparisons with empirical formula and experimental results of several different researchers show an acceptable accuracy of the proposed ANN model.

Keywords: bond; modelling; artificial neural network; compressive strength; relative rib area; cover

Mots-clés: Adhérence; modélisation; réseaux de neurones artificiels; résistance à la compression; aire relative des verrous; enrobage

1. Introduction

A fundamental property of reinforced concrete is the bond between the reinforcement and the concrete. In anchorage zones, the two important phenomena that control the bond are the force transfer mechanism between the reinforcement and the surrounding concrete and the capacity of the concrete to resist reinforcement pull-out. Chemical adhesion, friction and mechanical action are the mechanisms that assure bond efficiency. The contribution of each of these mechanisms depends on the surface and geometry of the reinforcement. In the case of ribbed bars, the force transfer is mainly governed by the blocking of the ribs in the concrete (Eligehausen & Bigaj van Vliet, 1999).

Bond failure of deformed bars normally involves the following phenomena (Tepfers, 1973): (1) local crushing of concrete in front of the bar ribs and/or (2) splitting of the concrete due to radial cracks around the bar. Local crushing dominates when the confinement provided by either surrounding concrete or transverse reinforcement is large and/or the rib height is small. This mechanism of bond failure tends to be ductile and does not cause much size effect. Splitting of the concrete dominates when the confinement is

*Corresponding author. Email: daoud_atef@yahoo.fr

© 2014 Taylor & Francis

small and/or the rib height is large. This mechanism is brittle and can be a significant cause of size effect. The size effect in bond has been illustrated directly or indirectly by several researchers. This size effect is mainly caused by the bar diameter, the cover thickness and the bar geometry (rib height). Many researchers discussed the theme of the size effect on the steel–concrete bond including (Bazant & Sener, 1988) size effect on pull-out test, (Soroushian & Choi, 1989) bar diameter, (Bamonte & Gambarova, 2007) effect of bar diameter on the bond stress versus slip curve in high-performance concrete, (Ichinose, Kanayama, Inoue, & Bolander, 2004) bar diameter and geometry, etc.

Thus, the bond strength depends on numerous and various factors, which basically concern the reinforcing bars, and the concrete and the stress state in both the reinforcing and the surrounding concrete (ACI, CEB-FIP, etc.).

Many researchers have brought up various formulae to estimate the bond strength of deformed steel reinforcement (Chapman & Shah, 1987; Harajli, 1994; Kemp, 1986; Orangun, Jirsa, & Breen, 1977). Of those, Orangun et al.'s equation serves as the basis for the ACI 318 building code on the development length. To date, most of the expressions for bond strength have these commonalities: they are empirical and based on statistics methodology. Thus, these equations are highly dependent on the test data used. Errors may be great if these equations are directly applied into different situations. Recently, (Torre-Casanova, Jasona, Davenne, & Pinelli, 2013) have proposed equations that distinguish splitting failure (function of the concrete tensile properties) and pull-out failure (function of the compressive concrete properties). In this study, only the cover-to-bar diameter ratio has been taken as parameter.

Analytical techniques have been very successful in the study of the behaviour of building materials. With the advent of digital computers, numerical methods have become much more attractive than the analytical solutions, as they can manage more complex and realistic situations. Numerical methods have their limitations as well because the number of variables that can be considered is still limited and numerical solutions cannot be obtained directly for occupant perceptions or preferences.

Many of the materials' problems are exactly the types of problems for which a connectionist approach, or neural network analysis, appears to be most applicable. In connectionist models of computation attempts are made to simulate the powerful cognitive and sensory functions of the human brain and to use this capability to represent and manipulate knowledge in the form of patterns. Based on these patterns, neural networks model input/output functional relationships and can make predictions about other combinations of unseen inputs. Neural networks have the potential for making better, quicker and more practical predictions than any of the traditional methods.

Artificial neural networks (ANN), a sub-field of artificial intelligence, are a family of parallel architectures that solve difficult problems via the cooperation of highly interconnected but simple computing elements or artificial neurons. Basically, the processing elements of a neural network are similar to the neurons of the brain, which consist of many simple computational elements arranged in layers (Yeh, 1998). Interest in neural networks has expanded rapidly in recent years. Much of the success of neural networks is due to such characteristics as non-linear processing and parallel processing. Recent researches are performed for the usability of ANN in civil engineering field, and especially for concrete technology (Subasi & Beycioglu, 2008). Lee (2003) utilised ANNs for the determination of concrete compressive strength. Lee (2003) suggested that ANN has a good predictive capacity. Topçu and Sarıdemir (2008) utilised ANN for determining the use of compressive strength of fly ash-added concretes. Topçu and Sarıdemir (2008) concluded that ANN method has high predictive performance. Altun, Kişi, and

Aydin (2008) used ANN and multiple linear regression techniques for the estimation of compressive strength of steel fibre-reinforced concrete. Dahou, Sbartaï, Castel, and Ghomari (2009) concluded that ANN can be used to model the experimental relationship between the ultimate pull-out load and bond strength. Elsanadedy, Al-Salloum, Abbas, and Alsayed (2012) used ANN and regression models for the prediction of strength parameters of FRP-confined concrete.

In this paper, bond strength and failure is investigated by conducting pull-out tests on ribbed bars with a nominal diameter of 12 mm. Various concrete covers were tested. Three bar types with different deformation pattern were investigated (French bar, Tunisian bar and Brazilian bar) and four concretes were studied. The effect of anchorage length has been also evaluated. The embedded length is limited to few bar diameters to prevent bar yielding (short anchorage).

Based on these experimental data, an ANN, a sub-field of artificial intelligence, was used in order to predict the ultimate pull-out load of the pull-out test specimen. An ANN model, with four inputs, was developed. Therefore, the ultimate pull-out load was the unique output data for the model.

2. Experimental programme

This investigation was designed to test the anchoring capacity of the reinforcement in the concrete. The cover thickness, concrete strength, embedment length and rib geometry or related rib area of pull-out test were considered as the main study parameters. Nominal bars of 12-mm diameter were selected to match typical main longitudinal steel. The study parameters were evaluated under monotonic loading in tension.

2.1. Test specimens

This investigation uses specimens in which a single reinforcing bar is embedded with a short anchorage length in a cylindrical plain concrete block. This short anchorage length provides a well-defined embedment length, prevents bar yielding and supports the assumption of uniform stress and deformation fields in the zone.

Figure 1 shows schematically a typical test specimen used in this investigation.

The pull-out specimens were cast in especially constructed forms with the reinforcing bar. The dimensions of tested specimen were 120 mm in length, and 5.52–13.3ϕ in diameter. The bond length is located at the top of the specimen and the rest of the specimen is debonded by the use of a small PVC pipe at the bottom of each specimen.

2.2. Concrete mixtures

The plain concrete mixture used without admixtures to cast the test specimens contained a normal Portland cement of type CEM I 42.5, the cement content ranged between 250 and 400 kg/m^3, and a water cement ratio, ranged between .45 and .90. The target compressive strengths for the concrete specimens ranged between 20 and 40 MPa. Local aggregates were used for the concrete mix design: 20 mm nominal maximum size crushed limestone and washed sand supplied by a local sand washing plant. The specimens were removed from their moulds 24 h after casting and stored and cured for 28 days at the concrete laboratory, and then were transferred to the structural laboratory for testing. Four different mix proportions of concrete are provided in Table 1.

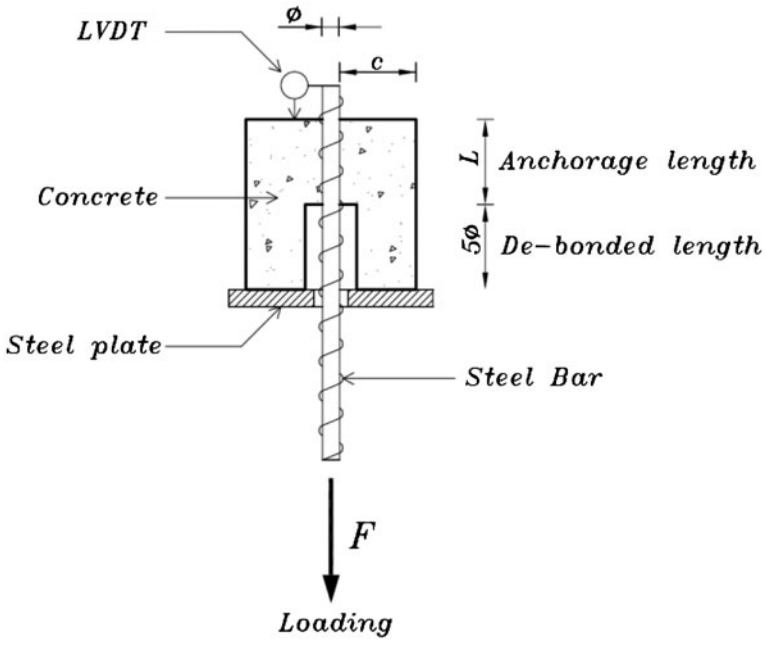

Figure 1. Specimen geometry and loading.

Table 1. Concrete mixture proportions.

	Quantity			
Material	C1	C2	C3	C4
CEM I 42.5 (kg/m^3)	400	400	315	250
Washed sand 0/4 (kg/m^3)	631.6	631.6	631.6	631.6
Crushed gravel 8/12 and 12/20 (kg/m^3)	1217.3	1217.3	1217.3	1217.3
Water (L)	180	220	220.5	225
W/C	.45	.55	.7	.9
Max. aggregate size (mm)	20	20	20	20
Mass per unit volume (kg/m^3)	2428.9	2468.9	2384.4	2323.9
Number of batches	1	5	1	1

The mechanical properties of the concrete are shown in Table 2, where f_c is the compressive strength and f_t is the tensile strength. The compressive tests were carried out conforming to EN 12390-3 standard and the tensile strength tests were performed in accordance with EN 12390-6 standard on cylindrical specimens of dimension 16 × 32 cm.

2.3. Reinforcement properties

Three types of steel bar, from three different continents, have been analysed in this study: a bar from Tunisia of nominal diameter 12 mm, a bar from France of nominal diameter 12 mm and a bar from Brazil of nominal diameter 12.5 mm.

Table 2. Mechanical properties of concretes.

Concrete	Compressive strength (MPa)	Brazilian tensile strength (MPa)
C1	42.8	3.34
C2-1	33.0	2.52
C2-2	36.8	2.96
C2-3	34.8	2.63
C2-4	34.2	2.89
C2-5	34.2	2.84
C3	26.3	2.28
C4	18.5	1.71

The surface roughness of each bar was characterised by the maximum height of profile calculated as the distance between the highest peak and the deepest valley on the bar surface.

For each bar, deformation height and spacing were measured at 10 locations on both sides of one bar, and the average relative rib areas were calculated using Equation (1). The details of the measurement and calculation of f_R are summarised in (Makni & Daoud, 2012). Parameters of f_R are given in Figure 2.

$$f_R = \sum_i \frac{A_r \sin(\beta_i)}{\pi \phi S_r} \tag{1}$$

where f_R corresponds to the related rib area; A_r is the surface of a rib; β is the angle between the rib and the longitudinal axis of the reinforcement; S_r corresponds to the spacing of the ribs; and ϕ is the external diameter of the deformed bar. The reinforcement properties, used in the tests, are summarised in Table 3.

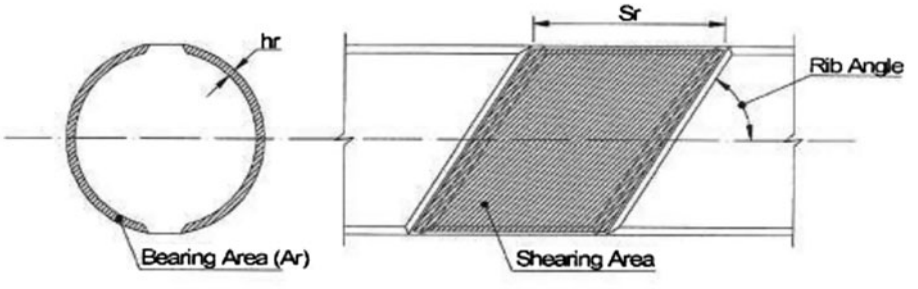

Figure 2. Parameters of the relative rib area f_R.

Table 3. Properties of the reinforcement bars.

Reinforcement	Nominal diameter ϕ (mm)	Related rib area f_R
From Tunisia	12	.084
From France	12	.070
From Brazil	12.5	.063

2.4. Pull-out test

The experimental set-up was inspired by the RILEM recommendations (RILEM, 1970). The pull-out specimens were tested in such a way that the concrete in the development region was not in compression. The reinforcing bar was pulled from one end of the test specimen while the other unloaded end was used to measure the bar slip.

A test frame was used to carry out the experimental programme. Some additional accessory parts were designed and fitted to facilitate the examination of bond strength investigation. A hydraulically controlled testing actuator with capacity of 300 kN was used to apply monotonic tensile load. The displacement was measured at the end of the unloaded steel bar by the use of the built-in Linear variable differential transducer with a 0–10 mm range secured in a tripod on the unloaded end of the specimen surface recorded bar slips that were archived electronically with the load readings. The typical loading rate was selected at 1.1 kN/s. All tests were run under load control until failure.

A total of 117 cylindrical pull-out specimens were tested within the current investigation; three replicate specimens were cast within a group. Only one parameter was changed at a time, while all other parameters were kept constant. For each test, the ultimate pull-out load is registered and the mode of failure is identified.

Table 4 shows the experimental plan of the pull-out test.

The bond strength was calculated assuming a uniform distribution of bond stresses along the bond length. It was calculated from the ultimate pull-out load as follows:

$$\tau_u = \frac{F_u}{\pi \cdot \phi \cdot L} \tag{2}$$

where τ_u is the ultimate average bond strength (MPa), ϕ is the reinforcement diameter (mm), L is the bond length (mm) and F_u is the ultimate pull-out load (N).

3. Experimental results

3.1. Pull-out load–slip curve

Figure 3 shows the typical experimental curve (pull-out load vs. slip) for pull-out failure obtained on the C2-5 concrete after 28 days with a 12.5 mm Brazilian steel bar, c/ϕ about 5.884 and 60 mm as an embedment length.

A typical load–slip curve for splitting failure is shown in Figure 4 for specimen from C2-2 concrete with 12 mm diameter as deformed bar from France, of 60 mm as embedment length and 2.375 of cover-to-bar diameter ratio.

The interaction between concrete and reinforcement is characterised by three different stages (FIB, 2000) (in the pre-pic zone because in our case all the tests are carried out in load control, which do not allow a good description of the post-pic behaviour of the interaction):

- Satge I (uncracked concrete): bond efficiency is assured mostly by chemical adhesion and no bar slip occurs but highly localised stresses arise close to lug tips.
- Stage II (first cracking): for higher bond stress, the chemical adhesion breaks down; in deformed bars the lugs induced large bearing stresses in the concrete and transverse microcracks originate at the tips of the lugs allowing the bar to slip but the wedging action of the lugs remains limited and there is no concrete splitting.

Table 4. Specimen parameters.

Specimens	f_{c28} (MPa)	ϕ (mm)	f_R	c (mm)	L (mm)	Number of replicate specimens
42-TN-60-2.375	42.8	12	.084	28.50	60	3
42-TN-60-3.417	42.8	12	.084	41.00	60	3
42-TN-604.458	42.8	12	.084	53.50	60	3
42-TN-60-5.083	42.8	12	.084	61.00	60	3
42-TN-60-6.150	42.8	12	.084	73.80	60	2
33-TN-60-2.375	33.0	12	.084	28.50	60	3
33-TN-60-3.417	33.0	12	.084	41.00	60	3
33-TN-60-4.458	33.0	12	.084	53.50	60	3
33-TN-605.083	33.0	12	.084	61.00	60	2
33-TN-60-6.150	33.0	12	.084	73.80	60	3
26-TN-60-2.375	26.3	12	.084	28.50	60	3
26-TN-60-3.417	26.3	12	.084	41.00	60	3
26-TN-60-4.458	26.3	12	.084	53.50	60	3
26-TN-60-5.083	26.3	12	.084	61.00	60	3
26-TN-606.150	26.3	12	.084	73.80	60	3
18-TN-60-2.375	18.5	12	.084	28.50	60	2
18-TN-60-3.417	18.5	12	.084	41.00	60	3
18-TN-60-4.458	18.5	12	.084	53.50	60	3
18-TN-60-5.083	18.5	12	.084	61.00	60	3
18-TN-60-6.150	18.5	12	.084	73.80	60	3
34-TN-90-2.375	34.2	12	.084	28.50	90	3
34-TN-90-3.417	34.2	12	.084	41.00	90	3
34-TN-90-4.458	34.2	12	.084	53.50	90	3
34-TN-90-5.083	34.2	12	.084	61.00	90	3
34-TN-90-6.150	34.2	12	.084	73.80	90	3
34-TN-40-2.375	34.8	12	.084	28.50	40	3
34-TN-40-3.417	34.8	12	.084	41.00	40	3
34-TN-40-4.458	34.8	12	.084	53.50	40	3
34-TN-40-5.083	34.8	12	.084	61.00	40	3
34-TN-40-6.150	34.8	12	.084	73.80	40	3
36-FR-60-2.375	36.8	12	.070	28.50	60	3
36-FR-60-3.417	36.8	12	.070	41.00	60	3
36-FR-60-4.458	36.8	12	.070	53.50	60	3
36-FR-60-5.083	36.8	12	.070	61.00	60	3
36-FR-60-6.150	36.8	12	.070	73.80	60	3
34-BR-60-2.260	34.2	12.5	.063	28.25	60	3
34-BR-60-3.260	34.2	12.5	.063	40.75	60	3
34-BR-60-4.260	34.2	12.5	.063	53.25	60	3
34-BR-60-4.860	34.2	12.5	.063	60.75	60	3
34-BR-60-5.884	34.2	12.5	.063	73.55	60	3

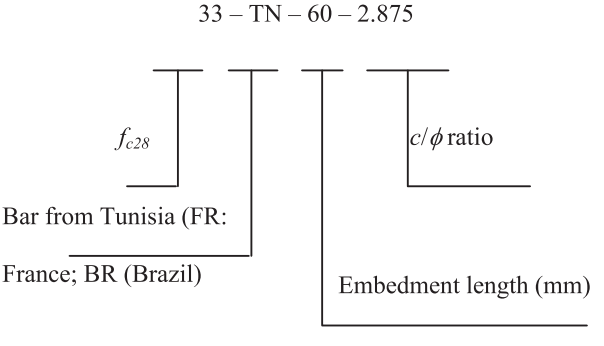

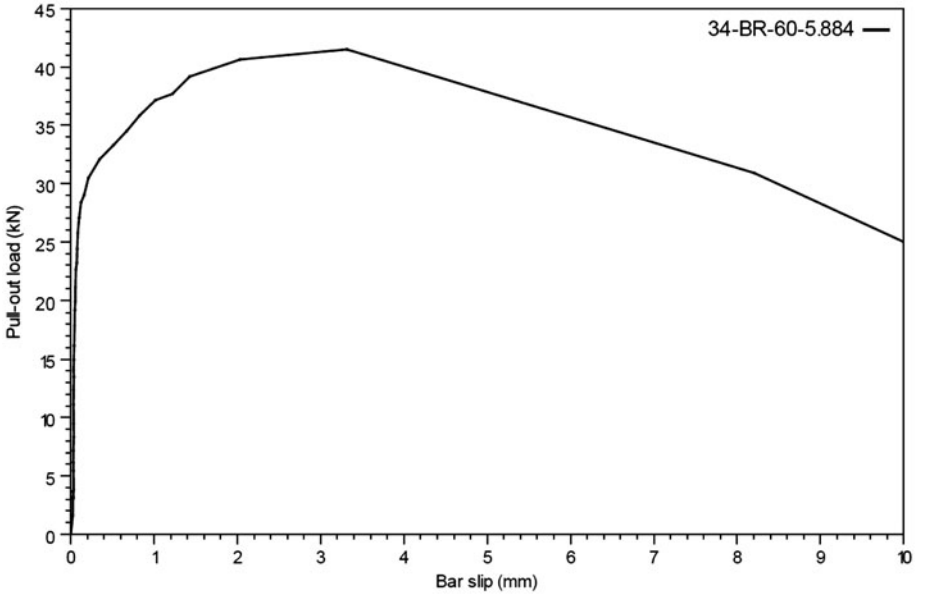

Figure 3. Pull-out load vs. bar slip for pull-out failure.

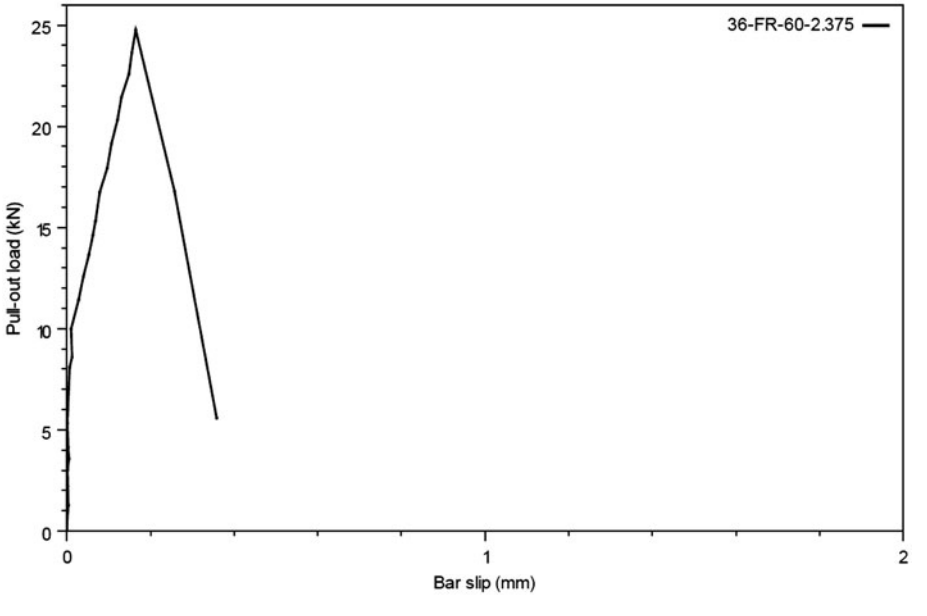

Figure 4. Pull-out load vs. bar slip for splitting failure.

- Stage III: the longitudinal cracks spread radially.
  - For a large cover (Figure 3): the surrounding concrete exerts a confinement action on the bar and bond strength and stiffness are assured mostly by the

concrete struts radiating from the bar and the undamaged outer ring. In this case, through splitting is prevented by their confining action and concrete splitting remains limited to a cracked core around the bar (pull-out failure).

- For a small cover (Figure 4): this stage ends as soon as concrete splitting reaches the outer surface of the concrete member. Afterwards, a more or less sudden failure occurs depending on the cover thickness. In this case, a sudden drop is observed because we have only 2.375 of cover-to-bar diameter ratio.

3.2. Effect of concrete compressive strength and related rib area on bond strength

Figure 5 presents the variation of average bond stress with c/ϕ ratio for different compressive strengths (specimen parameters: $L = 60$ mm and $f_R = .084$). We do not distinguish in this figure the failure mode. Figure 5 shows that regardless the specimen failure mode, for a given c/ϕ ratio bond, stress increases when the compressive strength of concrete increases.

For ribbed reinforcing bars, relative rib area plays an important role in bond strength. The bond strength with surrounding concrete is mainly controlled by the blocking of the ribs in the concrete. The failure is always due to the shearing-off of the concrete located between the consecutive ribs, which then depend on the concrete strength. The relative rib area f_R of the tested bars ranged from .063 to .084.

Figure 6 gives the variations of the average normalised bond stress with c/ϕ ratio for different relative rib areas. The use of the normalised bond stress is necessary to compare results from different compressive strength. Results show that, regardless of the failure mode of the specimen, related rib area influences significantly the bond stress.

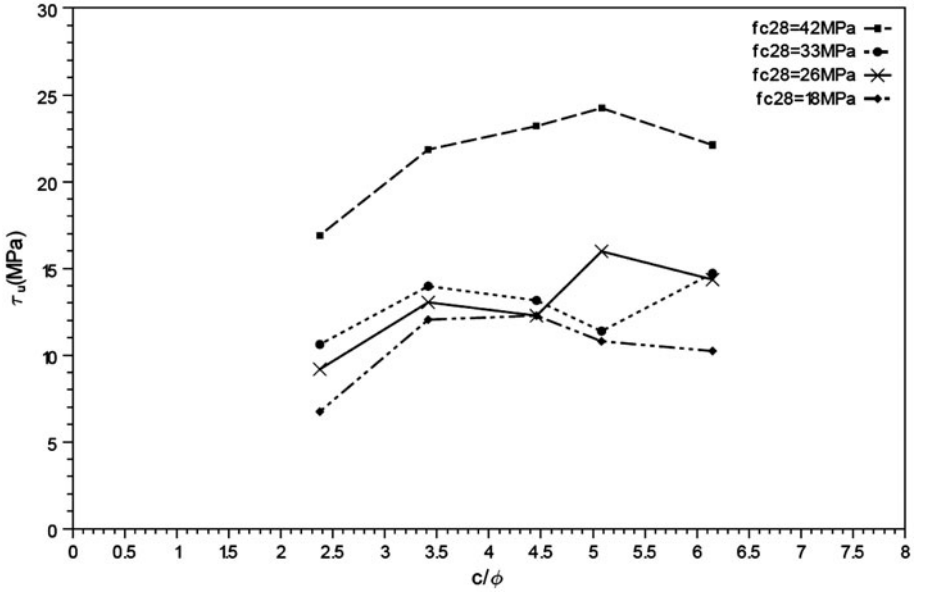

Figure 5. Variations of bond stress with c/ϕ ratio for $L = 60$ mm and $f_R = .084$: compressive strength effect.

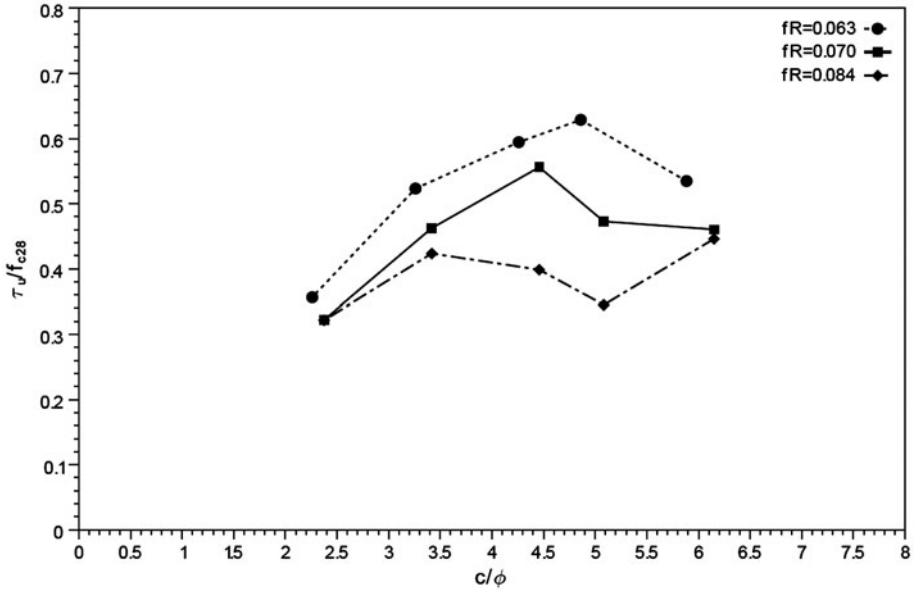

Figure 6. Variations of bond stress with c/ϕ ratio for $L = 60$ mm: effect of relative rib area.

3.3. *Effect of study parameters on bond failure*

Figure 7 presents the variation of $\frac{\tau_u}{f_{i28}}$ with c/ϕ ratio for all the experimental results. We distinguish in this figure only the failure mode of the specimen. The use of $\frac{\tau_u}{f_{i28}}$ ratio was initially used by Tepfers (1979) and recently by Torre-Casanova et al. (2013). Figure 7 shows that all the experimental results are within the upper (plastic solution) and the lower bound (partly cracked elastic solution) defined by Tepfers and that the variations seems to be in concordance with the numerical evolution proposed by (Torre-Casanova et al., 2013). However, experimental results show that there is a transition zone between splitting and pull-out failure (it ranges between $c/\phi = 4.0$ and 5.5). Indeed, there is no clear boundary and the transition zone depends on study parameters (f_{c28}, fR L).

3.4. *Synthesis and parameter of the ANN model*

Experimental results show that the concrete compressive strength, cover to bar diameter ratio, anchorage length and relative rib area have a significant effect on the ultimate pull-out load. Thus, the input data of the proposed ANN model must be selected to take into account the influence of these factors on the pull-out load, chosen as the output of the ANN modelling.

A data-set including 117 data samples obtained from experimental studies was used for ANN.

4. Neural network model development

ANN is a practice simulating the biological functioning of the human brain in order to imitate its reasoning capacities (Dreyfus et al., 2002; Jodouin, 1994). ANN can learn via trial and error, and so to generalise. In recent years, ANNs have shown exceptional performance as a regression tool, especially when used for pattern recognition and

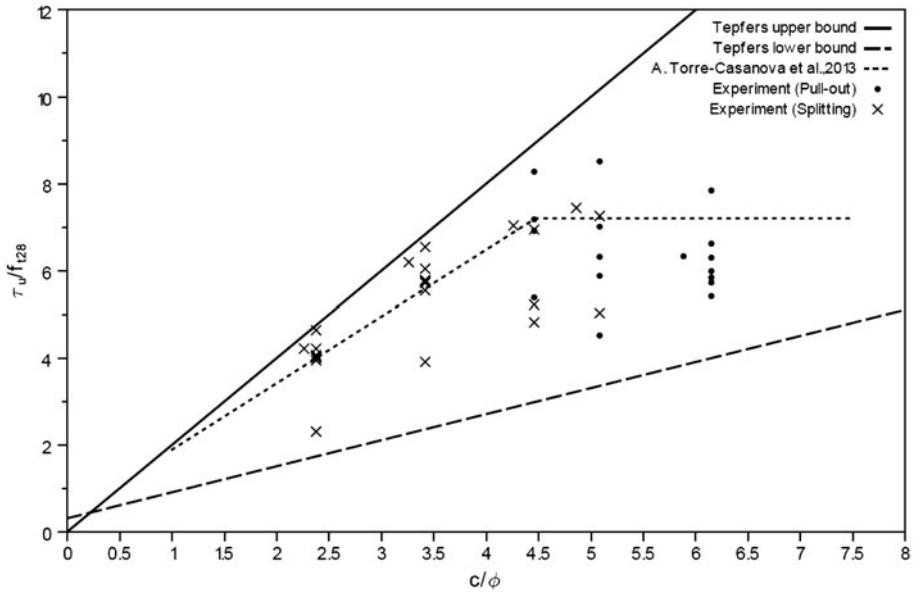

Figure 7. Variation of $\frac{\tau_u}{f_{t28}}$ with c/ϕ ratio: experimental results, upper (plastic solution) and the lower bound (partly cracked elastic solution) defined by Tepfers (1979).

function estimation (Erdem, 2010; Mukherjee & Biswas, 1997). They are highly non-linear and can capture complex interactions among input/output parameters in the system without any prior knowledge about the nature of these interactions. The principles of ANNs have been comprehensively discussed in detail elsewhere such as the history and theory of neural networks, and some indications of their future utility have been described in a plethora of published literature (Flood & Kartam, 1994). A very brief overview of how neural networks operate is presented in the following section.

The network consists of neurons in layers, each neuron being linked to a number of neurons in the subsequent layer. The training consists in adjusting the way a signal is processed in each connection when the signal passes through the network. A large network with many connections demands a high number of data-sets for training, whereas a smaller network can be trained satisfactorily with proportionally fewer data-sets. A typical ANN model is a combination of layers made of neurons. Most widely used ANN type is multi layer perception. Multi-layer perception (MLP) is composed of an input layer that takes the data in, an output layer that conveys the output of the network out and usually one but occasionally more than one hidden layer in between. In the input layer, input of the neurons are taken in from outside.

Figure 8 shows an MPL in which network input of a neuron in the hidden layers or the output layer is the sum of multiplications of all the input received (x_i) by corresponding weights (w_{ji}) while output of a neuron is got after the network input is processed by the activation function (Baillie & Mathew, 1994).

The relationship between the inputs and the output is given by the Equation (3).

$$Y_j = F(I) = F\left(b + \sum_{i=1}^{n} w_{ji}x_i\right) \tag{3}$$

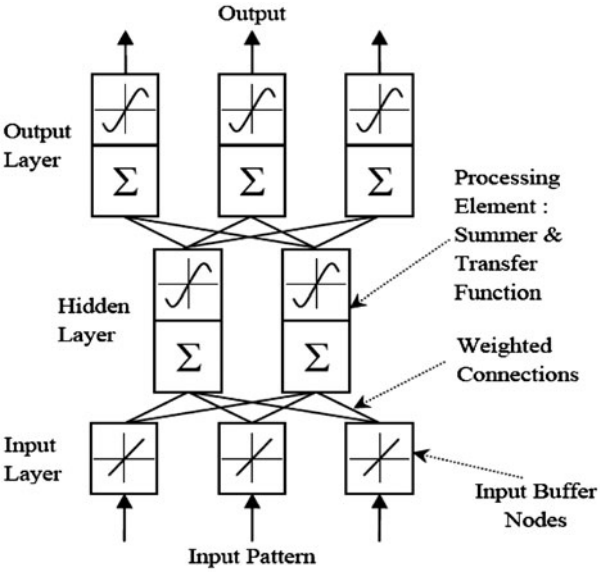

Figure 8. Architecture of a MLP (Baillie & Mathew, 1994).

where (n) is the total number of input neurons, (F) is the activation function, (x_i) is ith input variable, (w_{ji})s are weights for input between neuron i and j and b is the weight of the arc leading from the bias term. Each neuron is associated with a threshold value and an activation function. The activation function is used to compare the weighted sum of inputs and the threshold value of that neuron. If the threshold value is exceeded by the weighted sum the neuron goes to a higher state. Many different activation functions are used in different applications. Therefore, a sigmoidal activation function has been used here as follows (4):

$$Y_j = F(I) = \frac{1}{1 + e^{-\alpha(I-\theta_j)}} \tag{4}$$

where Y_j is the output of neuron j, I is the summation of all the weighted sums of the inputs for neuron j, θ_j is the threshold value of neuron j and α is a parameter which controls the slope of the activation function.

In the present study a back-propagation learning algorithm has been used to provide satisfactory results. This algorithm necessitates the use of a continuous, differentiable weighting function. The back-propagation learning is an iterated search process which adjusts the weights from output layer back to input layer in each run until no further improvement in Mean Square Error value is found. The back-propagation algorithm calculates the error, which is then used to adjust the weights first in the output layer, and then distributes it backward from the output to hidden and input neurons (Figure 9). This is done using the steepest gradient descent principle where the change in weight is directed towards negative of the error gradient.

The new weight is calculated as follows (5):

$$\Delta w_i = \alpha \Delta w_{i-1} - \eta \frac{\partial E_i}{\partial w} \tag{5}$$

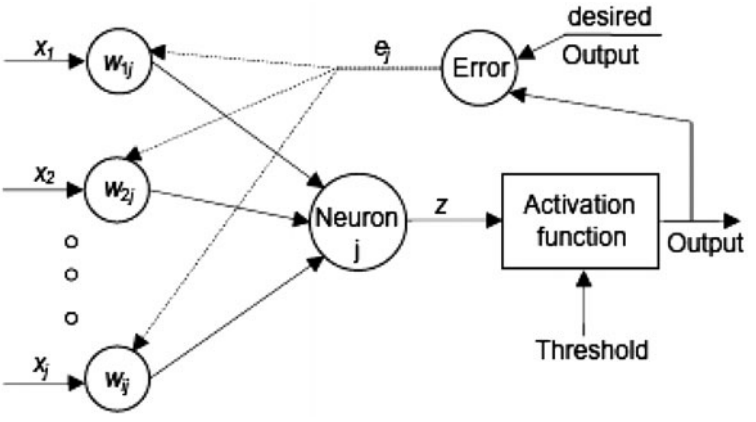

Figure 9. Neuron weight adjustment (Alshihri, Azmy, & El-Bisy, 2009).

where w is the weight between any two neurons; ∂w_i and ∂w_{i-1} are the changes in this weight at i and $i-1$ iteration; α is the momentum factor; and η is the learning rate.

E_i represents the root mean square error for iteration i as follows (6):

$$E_i = \sqrt{\frac{1}{N}\sum_{n=1}^{N}(e_n)^2} \qquad [6]$$

where e_n is the error between actual and predicted values, and N the total number of data points in validation.

In this present study, a BPANN with an MPL is proposed. ANN architecture used for this study is given in Figure 10. The computer program was performed under Matlab software using the neural toolbox. In the training, in order to avoid over-fitting of the network, the number of neuron of the unique hidden layer is equal to five, the sum

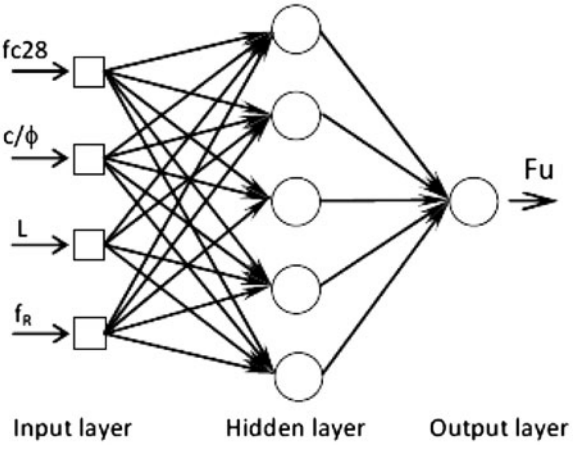

Figure 10. ANN pull-out model.

of input neuron and the output neuron (Braham & Hamblen, 1990; Hecht-Nielsen, 1991).

The database is divided into three subsets: training, testing and validation. To ensure statistical consistency of the subsets needed for the ANN model development, a random data division is used. About 70% of the total database was used for the training process, 15% for the testing and 15% for the validation.

The selections of the optimum network were deduced by the minimisation of the network error (Equation (5)).

The input layer weights (W), input layer biases (bh), hidden layer weights (Z) and hidden layer bias (b_0) of the optimum ANN model are given by Equations (7)–(10), respectively.

$$W = \begin{Bmatrix} .0068198 & -.15759 & -.84631 & -3.0598 \\ 1.1474 & -.98956 & .96489 & 1.6898 \\ -5.4218 & -1.4727 & -2.0244 & 1.9962 \\ 1.9219 & 1.6831 & -.63544 & .269 \\ -.97175 & 2.0855 & .22474 & 1.4179 \end{Bmatrix} \tag{7}$$

$$\text{bh} = \{\, .71526 \quad .52659 \quad -.40247 \quad .36281 \quad .35269 \,\} \tag{8}$$

$$Z \begin{Bmatrix} -2.665 \\ .68212 \\ 1.0941 \\ .68729 \\ 1.4915 \end{Bmatrix} \tag{9}$$

$$b_0 = \{-.052423\} \tag{10}$$

Figure 11 gives the experimental and the ANN model values of the pull-out test for all tested specimen. Predicted and measured values are presented in Figure 12. Figure 12 shows that predicted and measured ultimate pull-out loads are well correlated. The correlation coefficient R^2 is equal to .96. Moreover, 95% of the three subsets were located near the perfect prediction line with an absolute accuracy range of ±5 kN.

5. Validation of the ANN pull-out model on experimental results from the literature

In the literature there, are several analytical and numerical models which try to represent the bond stress response in the steel–concrete interface. In those models, most of them based in experimental results, several parameters were studied such as concrete compressive strength, concrete cover, steel bar diameter, embedment length and others. Several researchers have attempted to formulate equations that represent the bond between the reinforcing bars and concrete by means of linear or non-linear regressions from experimental results. Below is a brief description of a few:

- Orangun et al. (1977) and Harajli (1994) proposed the following formula:

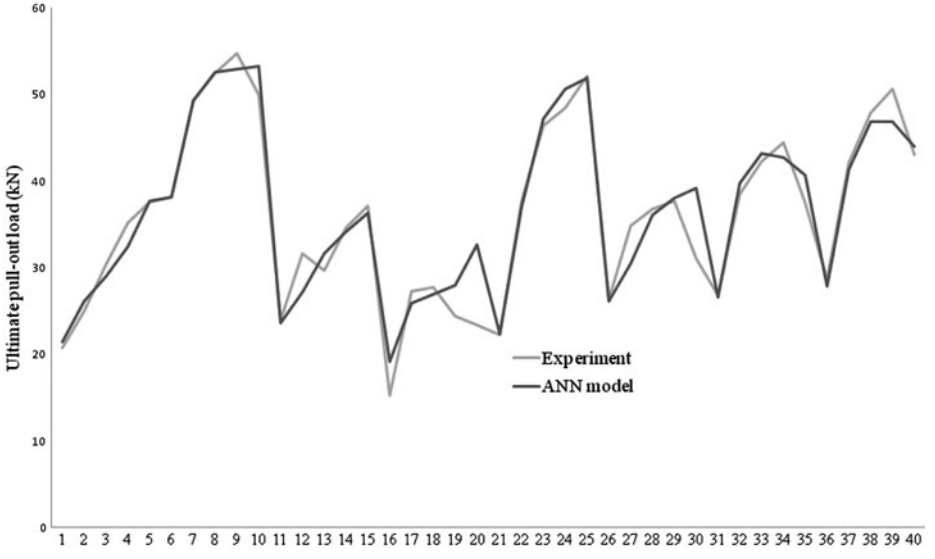

Figure 11. Comparison between experiment and ANN model for all the specimen.

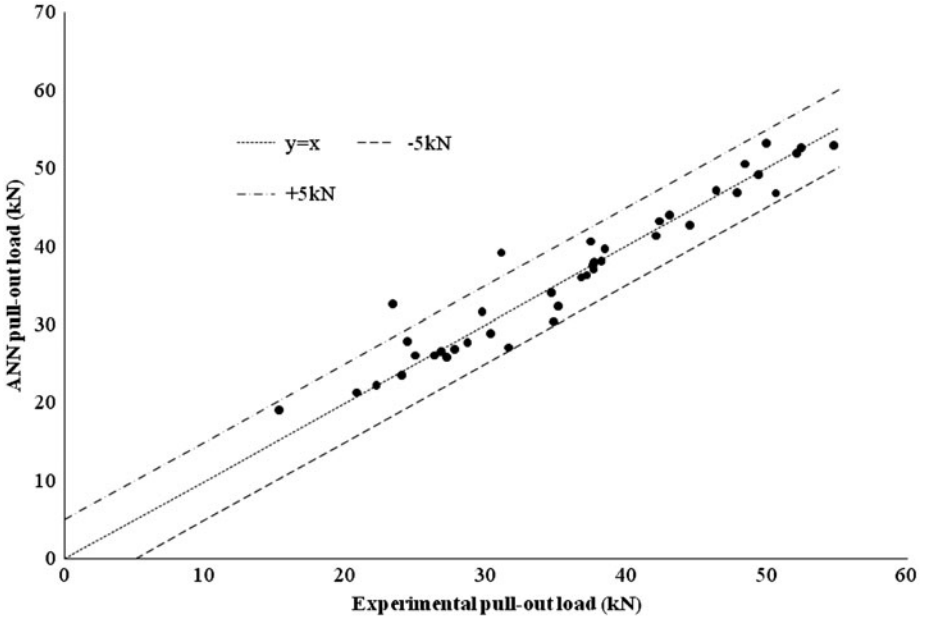

Figure 12. ANN-predicted vs. measured ultimate pull-out load data-set.

$$\tau_u = .083045\left[1.2 + 3\left(\frac{c}{\phi}\right) + 50\left(\frac{\phi}{L}\right)\right]\sqrt{f_c} \tag{11}$$

where c is minimum concrete cover, in mm, and f_c is the concrete compressive strength, in MPa.

- Chapman and Shah (1987) proposed another expression to predict bond strength as follows:

$$\tau_u = \left[3.5 + 3.4\left(\frac{c}{\phi}\right) + 57\left(\frac{\phi}{L}\right)\right]\sqrt{f_c} \tag{12}$$

where f_c is the concrete compressive strength, in Psi.

- Kemp (1986), describe the equation allow calculating the average bond strength from experimental hypothesis and recommended the following formula:

$$\tau_u = 232.2 + 2.716\left(\frac{c}{\phi}\right)\sqrt{f_c} \tag{13}$$

where f_c is the concrete compressive strength, in Psi.

- Al-Jahdali, Wafa, and Shihata (1994) proposed a modified expression (in SI) for bond strength as follows:

$$\tau_u = \left[-.879 + .324\left(\frac{c}{\phi}\right) + 5.79\left(\frac{\phi}{L}\right)\right]\sqrt{f_c} \tag{14}$$

Figures 13 and 14 show the variation of the bond strength versus the concrete compressive strength (f_c) and c/ϕ ratio of the above equations added with the ANN model results.

In Figure 13, the ANN model shows that bond stress increases with the increase of the compressive concrete strength. The variation is similar to the analytical equations proposed by the authors above. However, the ANN model results presented bond strength values higher than almost all equations predicted values bringing a safety response. The equation from Chapman and Shah had a good approach for the results of the ANN model.

Figure 14 shows that for all the authors above bond stress increases with the increase of c/ϕ ratio while the ANN model shows that bond stress increases for small values of c/ϕ ratio, and for large c/ϕ ratio bond stress is almost constant. This result shows that the larger the cover the smaller the role of c/ϕ ratio. This result is in concordance with the conclusion of (Torre-Casanova et al., 2013). Thus, the proposed model can distinguish between the pull-out failure and the splitting failure. Indeed, c/ϕ ratio has a small effect when the bond failure occurs by pull-out of the bar.

In order to check the validity of the proposed ANN model, experimental results obtained by other researchers were considered. Unfortunately, few results exactly fitting the variation range of our experimental input factors of the ANN model were available.

Table 5 shows concrete strength and specimen geometry parameters used by several different researchers and the ultimate bond stress measured experimentally. These parameters are used as input data for ANN model validation. In some cases, relative rib area value (f_R) is not mentioned by the authors. We take as input a mean value of the experimental range (.074).

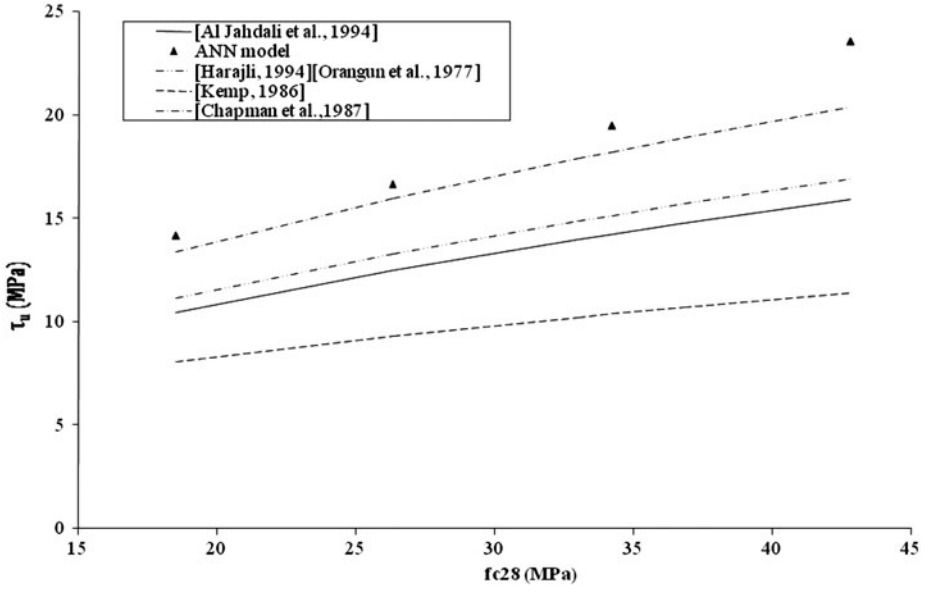

Figure 13. Bond strength vs. compressive strength for $L = 60$ mm and $c/\phi = 6.65$.

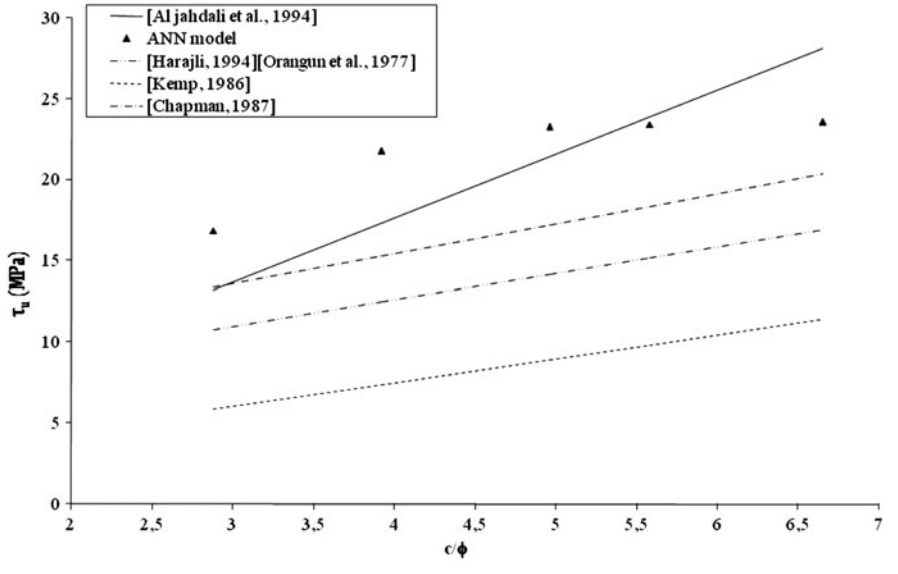

Figure 14. Bond strength vs. c/ϕ ratio for $f_{c28} = 42.8$ MPa and $L = 60$ mm.

The experimental and the predicted ultimate bond stress are then compared in Table 4. The ANN model reproduced the experimental ultimate bond stress with a maximal COV of 20%.

Table 5. Validation of the ANN model for ultimate bond stress prediction.

Ref.	f_c (MPa)	c/ϕ	L (mm)	f_R	Exp τ_u (MPa)	ANN τ_u (MPa)	COV
Castel, Vidal, Viriyametanont, and Raoul (2006)	34.4	6	60	.070	12.7	15.9	20.1
Daoud, Lorrain, and Elgonnouni (2002), Daoud (2003)	45	5	80	.079	15.1	15.2	.6
de Almeida et al. (2008)	30	5	80	.074	10.8	10.2	5.6

6. Conclusion

This paper presents a non-traditional approach to the prediction of the ultimate pull-out load based on ANN technique.

The pull-out tests were used to investigate some of the effect of the concrete strength, the cover thickness, the embedment length and the relative rib area.

The experimental results provided a database for implementing a neural network model for the ultimate pull-out prediction. The ANN model was developed with four inputs, compressive strength, c/ϕ ratio, embedment length and relative rib area. Values were analysed by means of multi-layer feed-forward back-propagation neural network model. In the analysis, gradient descent algorithm and one hidden layer was employed.

The following conclusions may be drawn from this study:

(1) The results show that ANN can be implemented to predict the ultimate pull-out load from compressive strength, c/ϕ ratio, embedment length and relative rib area.
(2) The model, trained, tested and validated according to the large database, shows good accuracy in the ultimate pull-out load prediction.
(3) Experimental results and ANN model exhibited good correlation with $R^2 = .96$; the proposed ANN is a valid alternative approach to prediction and programming using ANN.
(4) Comparisons with empirical formula and experimental results of several different researchers show an acceptable accuracy of the proposed ANN model.

References

Al-Jahdali, F. A., Wafa, F. F., & Shihata, S. A. (1994). Development length for straight deformed bars in high-strength concrete. *ACI Special Publication, SP-149*, 507–522.

Alshihri, M. M., Azmy, A. M., & El-Bisy, M. S. (2009). Neural networks for predicting compressive strength of structural light weight concrete. *Construction and Building Materials, 23*, 2214–2219.

Altun, F., Kişi, Ö., & Aydin, K. (2008). Predicting the compressive strength of steel fiber added lightweight concrete using neural network. *Computational Materials Science, 42*, 259–265.

Baillie, D., & Mathew, J. (1994). Diagnosis rolling element bearing faults with artificial neural network. *Acoustics Australia, 22*, 79–84.

Bamonte, P. F., & Gambarova, P. G. (2007, February). High-bond bars in NSC and HPC: Study on size effect and on the local bond stress-slip law. *Journal of Structural Engineering, 133*, 225–234.

Bazant, Z. P., & Sener, S. (1988). Size effect in pullout tests. *ACI Materials Journal, 85*, 347–351.

Braham, R., & Hamblen, J. O. (1990). The design of a neural network with a biologically motivated architecture. *IEEE Transactions on Neural Networks, 1*, 251–262.

Castel, A., Vidal, T., Viriyametanont, K., & Raoul, F. (2006). Effect of reinforcing bar orientation and location on bond with selfconsolidating concrete. *ACI Structural Journal, 103*, 559–567.

Chapman, R. A., & Shah, S. P. (1987). Early-age bond strength in reinforced concrete. *ACI Materials Journal, 84*, 501–510.

Dahou, Z., Sbartaï, Z. M., Castel, A., & Ghomari, F. (2009). Artificial neural network model for steel–concrete bond prediction. *Engineering Structures, 31*, 1724–1733.

Daoud, A. (2003). *Etude expérimentale de la liaison entre l'acier et le béton autoplaçant-Contribution à la modélisation numérique de l'adhérence* [Experimental study of the connection between steel and self-compacting concrete: Numerical contribution to the interface modelling] (Thèse de doctorat de l'INSA de Toulouse), p. 221. Toulouse, France: INSA.

Daoud, A., Lorrain, M., & Elgonnouni, M. (2002). Résistance à l'arrachement d'armatures ancrées dans du béton autoplaçant [Pull-out behaviour of reinforcement embedded in self-compacting concrete]. *Materials and Structures, 35*, 395–401.

de Almeida Filho, F. M., Debs, M. K., & El Debs, A. L. H. C. (2008). Bond-slip behavior of self-compacting concrete and vibrated concrete using pull-out and beam tests. *Materials and Structures, 41*, 1073–1089.

Dreyfus, G., Martinez, J. M., Samuelides, M., Gordon, M. B., Badran, F., Thiria, S., & Hérault, L. (2002). *Réseaux de neurones-Méthodologie et applications*. Eyrolles.

Eligehausen, R., & Bigaj van Vliet, A. (1999). Bond behaviour models. In *Fib Bulletin No. 1. Introduction-design process-materials* (Vol. 1, pp. 161–187). Lausanne, Switzerland: FBI.

Elsanadedy, H. M., Al-Salloum, Y. A., Abbas, H., & Alsayed, S. H. (2012). Prediction of strength parameters of FRP-confined concrete. *Composites Part B: Engineering, 43*, 228–239.

Erdem, H. (2010). Prediction of the moment capacity of reinforced concrete slabs in fire using artificial neural networks. *Advances in Engineering Software, 41*, 270–276.

Fédération Internationale du Béton (FIB). (2000). Bond of reinforcement in concrete. In *Bulletin No. 10, State-of-Art Rep. T.G. 4/2 Bond Models*. Lausanne, Switzerland: FIB.

Flood, I., & Kartam, N. (1994). Neural networks in civil engineering. I: Principles and understanding. *Journal of Computing in Civil Engineering, 8*, 131–148.

Harajli, M. H. (1994). Development/splice strength of reinforcing bars embedded in plain and fiber reinforced concrete. *ACI Structural Journal, 91*, 511–520.

Hecht-Nielsen, R. (1991). *Neurocomputing*. Reading, MA: Addison-Wesley.

Ichinose, T., Kanayama, Y., Inoue, Y., & Bolander, Jr, J. E. (2004). Size effect on bond strength of deformed bars. *Construction and Building Materials, 18*, 549–558.

Jodouin, J. F. (1994). *Les réseaux de neurones- principe et définitions* [Neural networks-principle and definitions]. Paris: Hermes.

Kemp, E. L. (1986). Bond in reinforced concrete: Behavior and design criteria. *ACI Journal, 83*, 50–57.

Lee, S. C. (2003). Prediction of concrete strength using artificial neural networks. *Engineering Structures, 25*, 849–857.

Makni, M., & Daoud, A. (2012). Caractérisation géométrique des barres d'acier pour béton armé par des méthodes expérimentales [Geometric characterization of steel bars for reinforced concrete by experimental methods]. *Annales de bâtiments et de travaux publics, 3–4*, 47–52.

Mukherjee, A., & Biswas, S. N. (1997). Artificial neural networks in prediction of mechanical behavior of concrete at high temperature. *Nuclear Engineering and Design, 178*, 1–11.

Orangun, C. O., Jirsa, I. O., & Breen, J. E. (1977). A reevaluation of test data on development length and splices. *ACI Journal, 74*, 114–122.

RILEM. (1970). Essai portant sur l'adhérence des armatures du béton : essai par traction [Bond test for reinforcing steel : pull-out test]. *Journal of Materials and Structures, 3*, 175–178.

Soroushian, P., & Choi, K. B. (1989). Local bond of deformed bars with different diameters in confined concrete. *ACI Structural Journal, 86*, 217–222.

Subasi, S., & Beycioglu, A. (2008). Determining the compressive strength of crushed limestone aggregate concrete using different prediction methods. *e-Journal of New World Sciences Academy, 3*, 580–589.

Tepfers, R. (1973). *A theory of bond applied to overlapped tensile reinforcement splices for deformed bars*, Publication 73:2. Goteborg: Division of Concrete Structures, Chalmers University of Technology.

Tepfers, R. (1979). Cracking of concrete cover along anchored deformed reinforcing bars. *Magazine of Concrete Research, 31*, 3–12.

Topçu, İ. B., & Sarıdemir, M. (2008). Prediction of compressive strength of concrete containing fly ash using artificial neural networks and fuzzy logic. *Computational Materials Science, 41*, 305–311.

Torre-Casanova, A., Jasona, L., Davenne, L., & Pinelli, X. (2013). Confinement effects on the steel–concrete bond strength and pull-out failure. *Engineering Fracture Mechanics, 97*, 92–104.

Yeh, I. (1998). Modeling of strength of high-performance concrete using artificial neural networks. *Cement and Concrete Research, 28*, 1797–1808.